Oxygen Surface Exchange Kinetics on Sr-Substituted Lanthanum Manganite and Ferrite Thin-Film Microelectrodes

Citation: la O', G. J., and Y. Shao-Horn. Oxygen Surface Exchange Kinetics on Sr-Substituted Lanthanum Manganite and Ferrite Thin-Film Microelectrodes. Journal of The Electrochemical Society 156, no. 7 (2009): B816. © 2009 The Electrochemical Society.

As Published: http://dx.doi.org/10.1149/1.3123214

Publisher: Electrochemical Society

Persistent URL: http://hdl.handle.net/1721.1/79366

Version: Final published version: final published article, as it appeared in a journal, conference proceedings, or other formally published context

Journal of The Electrochemical Society, **156** (7) B816-B824 (2009)
0013-4651/2009/156(7)/B816/9/$25.00 © The Electrochemical Society

Oxygen Surface Exchange Kinetics on Sr-Substituted Lanthanum Manganite and Ferrite Thin-Film Microelectrodes

G. J. la O' and Y. Shao-Horn[z]

Electrochemical Energy Laboratory, Massachusetts Institute of Technology, Cambridge, Massachusetts 02139, USA

The surface oxygen exchange kinetics occurring on dense $La_{0.8}Sr_{0.2}MnO_3$ (65 nm thick) and $La_{0.8}Sr_{0.2}FeO_3$ (110 nm thick) thin films were investigated by electrochemical impedance spectroscopy (EIS). Rutherford backscattering spectroscopy revealed that the bulk film compositions were consistent with the nominal stoichiometry, with $La_{0.8}Sr_{0.2}FeO_3$ having a slight Fe deficiency. Surface compositions of $La_{0.8}Sr_{0.2}MnO_3$ and $La_{0.8}Sr_{0.2}FeO_3$ were enriched in La using X-ray photoelectron spectroscopy and Auger electron spectroscopy. EIS data were utilized to determine the surface oxygen exchange coefficients, k^q and k_{chem}, in the range of temperatures from 790 to 660°C and oxygen partial pressures from 10^{-5} to 1 atm. The magnitudes of k^q and k_{chem} were found comparable for both $La_{0.8}Sr_{0.2}MnO_3$ and $La_{0.8}Sr_{0.2}FeO_3$, and a P_{O_2} dependence m fell in the range from ~0.2 to ~0.3. The thermodynamic enhancement factor γ was consistently higher for $La_{0.8}Sr_{0.2}MnO_3$ than $La_{0.8}Sr_{0.2}FeO_3$, which was in reasonable agreement with estimates based on thermogravimetric data of powder materials reported previously. The chemical capacitance for $La_{0.8}Sr_{0.2}FeO_3$ was approximately 1 order of magnitude larger than $La_{0.8}Sr_{0.2}MnO_3$, which indicates a larger oxygen vacancy content. The rate-limiting steps of surface oxygen exchange on $La_{0.8}Sr_{0.2}MnO_3$ and $La_{0.8}Sr_{0.2}FeO_3$ were discussed with regard to previously proposed models.
 [DOI: 10.1149/1.3123214]

Manuscript submitted January 26, 2009; revised manuscript received March 26, 2009. Published May 11, 2009.

Surface oxygen exchange and diffusion of oxygen ions are the two key processes that control the oxygen reduction reaction (ORR) through mixed ionic and electronic conducting (MIEC) cathodes. The diffusion of oxygen in the lattice of many perovskite-based MIECs is relatively well characterized due to the tremendous technological implications for these in applications such as oxygen separation membranes, solid oxide fuel cell (SOFC) cathodes, and gas sensors, to name a few.[1-7] However, below a critical thickness L_c,[8] defined as the ratio of the oxygen diffusion coefficient (D in cm^2/s) and the surface oxygen exchange coefficient (k in cm/s) (where $L_c = D/k$), surface exchange will start to limit ORR kinetics, where any further reduction of MIEC cathode thickness would provide no additional enhancement. Surface oxygen exchange on oxides is poorly understood. A variety of techniques had been used to quantify k and D and determine L_c such as (*i*) ^{18}O tracer gas for ion exchange depth profile (IEDP) with secondary-ion mass spectrometry (SIMS),[2,3,7,9] (*ii*) conductivity relaxation methods,[4,10,11] (*iii*) oxygen permeation studies,[6,12] and, more recently, (*iv*) electrochemical impedance spectroscopy (EIS).[13,14] A number of earlier studies using IEDP/SIMS techniques have shown empirical correlations of tracer surface oxygen exchange (k^*) with oxygen tracer diffusion coefficient (D^*), which suggests the importance of oxygen vacancies for oxygen exchange.[2,7,9,15] However, the influence of oxygen vacancies on k^* is shown to be much smaller than that on D^* because k^* values of MIEC cathodes[16,17] such as $La_{1-x}Sr_xFe_{1-y}Co_yO_{3-d}$ (LSCF) and $La_{1-x}Sr_xMnO_3$ (LSM)[2,3,18] differ by 1–2 orders of magnitude, while D^* of LSM is 4–5 orders of magnitude lower than that of MIEC cathodes. More recently, De Souza[19] proposed that the availability of electronic species governs the rate of oxygen surface exchange, where low concentrations of oxygen vacancies and high concentrations of charge carriers are needed for high exchange rates. This previous model[19] is largely in agreement with mechanisms reported by Adler et al.,[20] where a metallic band structure is considered important in surface oxygen exchange. Using this concept, one would expect that the surface exchange rate on LSM with higher electronic conductivity[21] but lower oxygen ion conductivity[2,22] is higher than that on $La_{1-x}Sr_xFeO_{3-d}$ (LSF). The focus of this study is to examine and compare the kinetics of surface oxygen exchange of LSM and LSF as a function of oxygen partial pressure (P_{O_2}) and temperature.

For materials with very poor oxygen diffusion and limited oxygen nonstoichiometry in bulk, such as LSM, significant challenges remain in accurately measuring k^* and P_{O_2} dependence, particularly at P_{O_2} levels relevant to SOFC cathode operation. Using IEDP/SIMS, the ^{18}O isotope fractions in the gas phase approach those on the surface of the LSM cathode, which results in large errors of 2 orders of magnitude or more in fitting k^* at P_{O_2} of $>10^{-3}$ atm.[2,19] For oxygen permeation studies, given the extremely small L_c for LSM,[2] estimated to be ~10 nm at 720°C (using $D^* \sim 10^{-14}$ cm^2/s and $k^* \sim 10^{-9}$ cm/s), the fabrication of sub-100 nm freestanding membranes poses a significant challenge.[23] An alternative method demonstrated by Jacobson and co-workers[13,14] and by Maier[24] is to determine the chemical surface oxygen exchange coefficient (k_{chem}) and the electrical surface oxygen exchange coefficient (k^q) from EIS measurements that is approximately equivalent to k^* from tracer experiments.[25] In this study, we examine the surface oxygen exchange kinetics on $La_{0.8}Sr_{0.2}MnO_3$ (LSM80-20) and $La_{0.8}Sr_{0.2}FeO_3$ (LSF80-20) thin-film microelectrodes using EIS. The chemical compositions on the surface of these microelectrodes is determined using Auger electron spectroscopy (AES) and X-ray photoelectron spectroscopy (XPS), while the bulk composition is analyzed using Rutherford backscattering spectroscopy (RBS). Surface exchange rates of k^q and k_{chem} of LSM80-20 obtained from EIS measurements are comparable to those of LSF80-20, from which insights into the influence of electronic properties and oxygen vacancies on the surface exchange rate is discussed.

In this study, it is of great interest to compare the P_{O_2} dependence on the surface exchange rates of LSM80-20 and LSF80-20. Ambiguities exist in the rate-limiting step for surface oxygen exchange in the literature, which is largely derived from experimentally observed P_{O_2} dependence on surface exchange rates. Three different rate-limiting steps for surface oxygen exchange have been reported for perovskites. De Souza[19] suggested that the rate-limiting step involves the combination of atomic oxygen species and electrons (charge transfer) for both electron-poor and electron-rich perovskites. Adler and co-workers[20] reported that a dissociative adsorption step was the rate-limiting step for metallic $La_{1-x}Sr_xCoO_{3-d}$ (LSC), while chemisorption was the rate-limiting step for p-type semiconductor LSF. More recently, Fleig et al.[26] showed that electron-transfer steps such as $O_{ad} + e^- \rightarrow O_{ad}^-$ and $O_{ad}^- + e^- \rightarrow O_{ad}^{2-}$ can be the rate-limiting step on materials with P_{O_2}-independent hole concentrations and materials having electronic carrier concentrations with P_{O_2} dependence of $\frac{1}{4}$, in the P_{O_2} and temperature relevant to SOFC operation (from 10^{-5} to 1 atm at

[z] E-mail: shaohorn@mit.edu

1000 K). In this study, we found that the P_{O_2} dependences for k^q and k_{chem} of LSM80-20 and LSF80-20 are similar, in the range from ~0.2 to ~0.3. The results are discussed in the context of previous models described above, from which are provided some insights into the rate-limiting step for surface oxygen exchange on perovskite materials.

Experimental

An 8 mol % yttria-stabilized zirconia (YSZ) electrolyte (Praxair Specialty Ceramics, USA) was initially sputtered onto alumina (Al_2O_3) substrates for 3 h at 400 W with an argon (Ar) to oxygen (O_2) atmosphere ratio of 7.5:1. The deposited films were then annealed in air at 800°C for 3 h. Cathode targets with LSM80-20 composition were deposited subsequently on top of the YSZ film by sputtering at 300 W, with the substrate heated to ~550°C under an identical Ar to O_2 ratio, from which LSM80-20 films with a thickness of 65 nm were obtained. Pulsed laser deposition was used to deposit LSF80-20 from a 1 in. diameter target (Praxair Specialty Ceramics, USA) on top of YSZ. The LSF80-20 films with a thickness of 110 nm were obtained after a deposition of 2 h using an excimer laser operating at a wavelength of 248 nm, a 10 Hz repetition rate, an energy of 500 mJ/pulse, and a substrate heating at 800°C. LSM80-20 and LSF80-20 film thickness was verified using a DekTak profilometer (Veeco, USA). LSM80-20 and LSF80-20 microelectrodes were then completed using photolithography and acid etching to remove excess LSM80-20 and LSF80-20. Platinum (Pt) counter electrodes were subsequently sputter deposited adjacent to the LSM80-20 and LSF80-20 microelectrodes for 20 min at 100 W power in pure Ar atmosphere. Excess Pt was removed by photoresist lift-off using acetone. Further details on the fabrication, photolithography, and characterization of the thin-film microelectrodes are found in a previous study.[27]

Fabricated thin films were examined using optical microscopy (Mitutoyo FS-70, Kawasaki, Japan) and scanning electron microscopy (SEM) (FEI/Philips XL30 FEG ESEM, Oregon). Phase analysis was conducted by X-ray diffraction (XRD) collected using a Bruker D8 (Karlsruhe, Germany) multipurpose diffractometer with a copper anode (Cu Kα) using a 0.5 mm beam monochromator. The beam monochromator was positioned 15 cm from the sample, resulting in a 2θ frame width of 15° and a fixed incident angle of 10°. A scan rate of 60 s/frame was used in the 2θ from 20 to 65°. All diffraction patterns were analyzed using the Jade software package (Materials Data, Inc., Version 7).

The surface chemical compositions of the samples were measured using AES and XPS. LSM80-20 and LSF80-20 thin films were examined in the "annealed" state (800°C for 10 h and slowly cooled at a rate of 5°C/min to room temperature). Patterned microelectrodes of identical samples were, in contrast, examined in the "quenched" state after heating the annealed sample to ~700°C and quenching from ~700°C to room temperature in <5 s. AES was performed on a Physical Electronics model 660 scanning Auger microscope (Chanhassen, MN) with a lanthanum hexaboride (LaB_6) filament operating at an accelerating voltage of 10 kV. Analysis areas were limited to a 10 × 10 μm dimension on the LSM microelectrodes. In AES, the obtained energy spectrum for a particular element is always situated on a large background (low signal-to-noise ratio), which arises from the vast number of so-called secondary electrons generated by a multitude of inelastic scattering processes. To obtain better sensitivity for the detection of the elemental peak positions, the AES spectra from this study were presented in the differentiated form. Elemental quantification of AES spectra utilized relative sensitivity factors (RSFs) of 0.019, 0.027, 0.161, and 0.212 for La_{MNN}, Sr_{LMM}, Mn_{LMM}, and O_{KLL}, respectively, as supplied by the AES manufacturer (Physical Electronics). XPS was performed on a Kratos Axis Ultra spectrometer (Manchester, U.K.) with a monochromatized aluminum X-ray source (Al Kα). The analysis area was set to a minimum size of 1.1 mm diameter spot, and survey spectra were initially collected at low resolution. Higher resolution spectra were then obtained for quantitative analysis of elemental contents of LSM80-20 and LSF80-20, with each spectrum consisting of at least 20 cycles. To compensate for sample charging effects, all spectra were calibrated with the carbon (C) 1s photoemission peak for adventitious hydrocarbons at 284.6 eV. RSF values of 9.122, 1.843, 2.659, and 0.78 for La_{3d}, Sr_{3d}, Mn_{2p}, and O_{1s}, respectively, were utilized as supplied by the XPS manufacturer (Kratos Analytical). RBS (Evans Analytical Group, Sunnyvale, CA) was performed on annealed LSM80-20 films to determine the elemental composition of the entire film using a He^{2+} ion beam with 2.275 MeV energy and a detector angle of 160° for the normal angle and a shallow grazing angle of 112°.

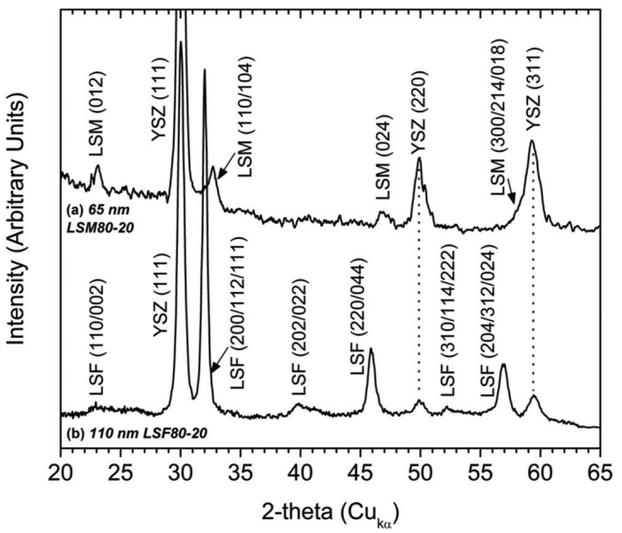

Figure 1. XRD patterns from an annealed (a) 65 nm thick LSM80-20 film and (b) 110 nm thick LSF80-20 film. Both samples were supported on YSZ electrolyte and single phase. X-ray patterns were collected in the glancing angle mode with an incident angle of 10°.

EIS measurements of annealed microelectrodes from ~130 to ~ 190 μm were performed using a microprobe station (Karl Suss, Germany) equipped with an optical microscope (Mitutoyo FS-70, Japan) and a temperature-controlled heating stage (Linkam TS1500, U.K.). The microelectrodes were contacted by Pt-coated, tungsten carbide probes having a radius of 7 μm. EIS measurements were conducted with a Solartron 1260 frequency response analyzer connected to a Solartron 1296 dielectric interface. EIS data were collected in the frequency range from ~1 MHz to ~ 100 μHz using an ac voltage amplitude of 10 mV in the temperature range of 770–570°C in air. Actual microelectrode surface temperatures were calibrated using a thermocouple contacting the thin-film surface to have a deviation of ±5°C for each temperature setpoint. EIS experiments to probe surface exchange were carried out under varying nitrogen (N_2) to O_2 mixtures with a P_{O_2} range of 10^{-5}–1 atm. ZView software (from Scribner Associates, USA) was used to construct the equivalent circuit and perform a complex least-squares fitting to deconvolute the impedance response and extract resistance and capacitance values of different processes.

Results and Discussion

Crystal structure, surface microstructure, and chemical compositions.— XRD results showed that both LSM80-20 and LSF80-20 films were crystalline and single phase after annealing, as shown in Fig. 1. LSM80-20 films had a perovskite structure with rhombohedral symmetry (space group $R\bar{3}c$) and slight peak shifts toward higher 2θ angles, which indicates changes in the lattice parameters of $\Delta a = -0.340\%$ and $\Delta c = +0.325\%$ ($a = b = 5.51$ Å, c

Table I. Elemental atomic concentration (%) of La, Sr, Mn, and Fe from the surface of LSM80-20 and LSF80-20 thin films as obtained from XPS, AES, and RBS analyses.

		Annealed samples (annealed at 800°C for 10 h)				Quenched samples (annealed at 800°C and quenched)	
		RBS		XPS		AES	
Atomic concentration (%)	Nominal composition	LSM80-20	LSF80-20	LSM80-20	LSF80-20	LSM80-20	LSF80-20
La	16	15.5	17.5	13.2	20.1	43.6	37.8
Sr	4	5.5	5.0	1.9	3.9	4.5	9.3
Mn/Fe	20	20.0	15.0	3.0	5.5	5	15.7
O	60	59.0	62.5	81.8	70.5	46.8	37.2
Cations only[a]	$La_{0.80}Sr_{0.20}(Fe/Mn)_{1.0}$	$La_{0.80}Sr_{0.28}Mn_{1.03}$	$La_{0.80}Sr_{0.23}Fe_{0.69}$	$La_{0.80}Sr_{0.12}Mn_{0.18}$	$La_{0.80}Sr_{0.16}Mn_{0.22}$	$La_{0.80}Sr_{0.08}Mn_{0.10}$	$La_{0.80}Sr_{0.20}Mn_{0.33}$

[a] Normalizing with nominal La content of 0.8.

= 13.41 Å, and V = 352.68 Å^3) in comparison to the stoichiometric compound.[28] Some preferred orientation was noted for the (012) Bragg reflection, which was equivalent to the (100) plane in the cubic perovskite structure. The XRD analysis of LSF80-20 revealed that the expected orthorhombic structure (space group *Pbnm*) has slight peak shifts to higher 2θ angles, which indicates changes in the lattice parameters of Δa = + 0.540%, Δb = −0.690%, and Δc = + 0.969% (a = 5.58 Å, b = 5.47 Å, c = 7.92 Å, and V = 243.31 Å^3) in comparison to the stoichiometric reference compound.[29] A preferred orientation was also observed for the (200) Bragg reflection of LSF80-20. XRD peaks of the YSZ films after annealing (space group $Fm\bar{3}m$, a = 5.160 Å, and V = 137.39 Å^3) were in good agreement with those of the YSZ sputtering target and YSZ listed in the Joint Committee on Powder Diffraction Standards.[30] Interatomic distances in the (012) plane of LSM80-20 were ~6% larger than those of YSZ (110), while interatomic distances in the (200) planes of LSF80-20 were ~6% larger than those of YSZ (110). Bulk elemental analysis results using RBS on LSM80-20 and LSF80-20 are summarized in Table I. The RBS analysis of sputtered and annealed LSM80-20 revealed a bulk composition of La 15.5 ± 1 atom %, Sr 5.5 ± 1 atom %, Mn 20 ± 2 atom %, and O 59 ± 6 atom %, which was close to the nominal stoichiometry of La 16 atom %, Sr 4 atom %, Mn 20 atom %, and O 60 atom %. The RBS analysis on laser-ablated and annealed LSF80-20 revealed a bulk composition of La 17.5 ± 1 atom %, Sr 5.0 ± 1 atom %, Fe 15.0 ± 2 atom %, and O 62.5 ± 6 atom %, which contained some Fe deficiencies in comparison to the nominal composition of La 16 atom %, Sr 4 atom %, Fe 20 atom %, and O 60 atom %. Therefore, a higher 2θ peak shifting for both LSM80-20 and LSF80-20 may arise from (*i*) compressive strains associated with partial coherency between LSM80-20 or LSF80-20 and YSZ surfaces, and (*ii*) LSF80-20 deviation from nominal stoichiometry.

SEM and atomic force microscopy (AFM) analyses of LSM80-20 and LSF80-20 microelectrodes revealed that they were dense and crack-free before EIS testing, as shown in Fig. 2a-d. AFM analysis revealed smooth LSM80-20 sputtered surfaces with root-mean-square (rms) surface roughness of ~3 nm in the quenched sample, as shown in Fig. 2b. AFM analysis on LSF80-20, presented in Fig. 2d, revealed a similar smooth surface with rms surface roughness of ~8 nm.

Surface elemental analysis results using XPS and AES on LSM80-20 and LSF80-20 are summarized in Table I. Surface analysis using XPS of annealed LSM80-20 films, in contrast, revealed significant La enrichment with a cation chemical formula of $La_{0.80}Sr_{0.12}Mn_{0.18}$ after normalizing with a nominal La content. AES analysis of LSM80-20 after annealing and quenching revealed a similar La enrichment with a cation chemical formula of $La_{0.80}Sr_{0.08}Mn_{0.10}$. Both XPS and AES revealed that the surface La/Sr and La/Mn ratios were higher than the nominal LSM80-20 composition. The XPS analysis of annealed LSF80-20 also showed significant La enrichment with a cation stoichiometry of $La_{0.80}Sr_{0.16}Fe_{0.22}$ after normalizing with a nominal La content. The AES analysis of annealed and quenched LSF80-20 showed a similar La enrichment with a cation stoichiometry of $La_{0.80}Sr_{0.20}Fe_{0.33}$ from nominal LSF80-20. These surface analysis results represented almost nominal La/Sr ratios. However, the surface La/Fe ratio was higher than the nominal LSF80-20 composition. Evidence of La surface segregation found in this study was in agreement with the study by Baumann et al.,[31] which showed La/(Co + Fe) and La/Sr atomic concentration ratios that were higher than nominal ratios on the surface of dense LSCF thin-film microelectrodes. The selection of RSF factors for La, Mn, and Sr in the elemental quantification of XPS and AES data may influence the extent of surface La enrichment and Mn deficiency determined from these techniques. These

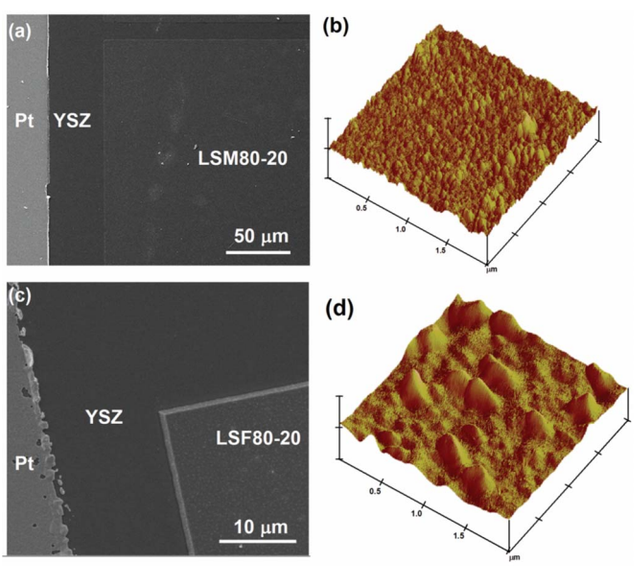

Figure 2. (Color online) SEM and AFM of dense and patterned films of [(a) and (b)] sputtered LSM80-20 and [(c) and (d)] laser-ablation-deposited LSF80-20 after quenching at ~700°C. Both electrodes were fully dense and crack-free before and after electrochemical testing. AFM images are shown with a maximum height of 70 nm. AFM measurements revealed the LSM80-20 and LSF80-20 films' surface rms roughness of ~3 and ~8 nm, respectively.

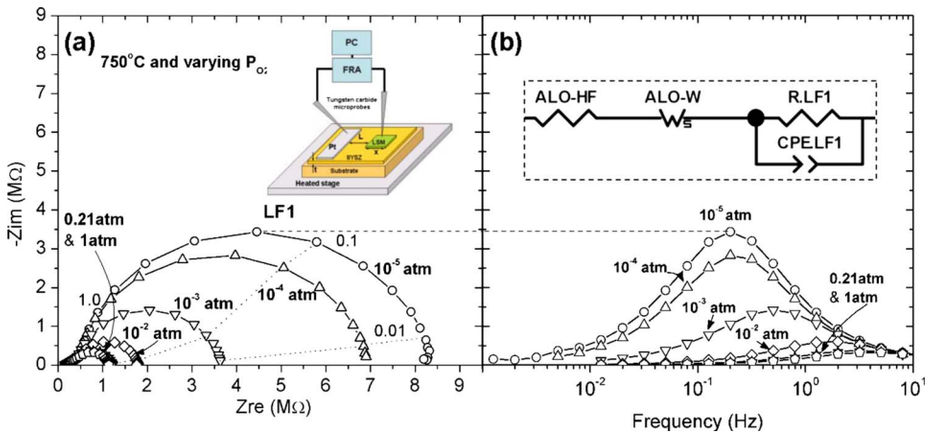

Figure 3. (Color online) (a) Typical EIS spectra at 750°C from LSM80-20 microelectrode, ~190 μm in size and 65 nm thick, showing the variation of impedance with different P_{O_2} from 10^{-5} to 1 atm at 750°C. The in-plane testing configuration is shown in the inset. (b) Plot of $-Z_{im}$ vs frequency showing the change in peak frequency as a function of P_{O_2}. At P_{O_2} = 1 atm, the peak frequency approaches 5 Hz. At $P_{O_2} = 10^{-5}$ atm, the peak frequency approaches 20 mHz. The equivalent circuit used to deconvolute the single-semicircle impedance spectra is shown in the inset.

correction factors are being calibrated with single-crystal, stoichiometric LSM80-20 thin films, which will be reported in future studies.

ORR impedance data of LSM80-20 and LSF80-20 microelectrodes.— The LSM80-20 microelectrodes were tested using an in-plane configuration, as shown in the schematic in Fig. 3a inset. Typical EIS data from LSM80-20 microelectrodes with a thickness of 65 nm at 750°C showed one low frequency semicircle, identified as LF1, and the impedance of LF1 decreasing with increasing P_{O_2} from 10^{-5} to 1 atm, as shown in Fig. 3a. A shift in the peak frequency from ~5 Hz at P_{O_2} = 1 atm to ~ 20 mHz at P_{O_2} = 10^{-5} atm was observed in the plot of the imaginary impedance ($-Z_{im}$) as a function of frequency, as presented in Fig. 3b. An equivalent circuit presented in Fig. 3b inset with resistors ($R_{ALO\text{-}HF}$, R_{LF1}), finite-length Warburg ($W_{ALO\text{-}W}$), and constant-phase elements (CPE_{LF1}) was used to deconvolute the impedance response as a function of P_{O_2} and temperature. The ORR impedance (LF1 impedance) was found to increase with decreasing P_{O_2}, which suggests that the kinetics of ORR was limited by surface chemical processes such as surface oxygen exchange.[32] Although previous IEDP/SIMS studies of LSM80-20 micrometer-sized particles suggested that the critical thickness for surface-controlled ORR, L_c, is ~10 nm at 720°C,[2,7] our recent studies[27,33] showed that the impedance associated with the three-phase boundary/bulk charge transfer vanishes at the microelectrode thickness of 65 nm at 750°C. Our findings were in agreement with those of Fleig et al.,[34] where a critical thickness of ~200 nm was recently extrapolated for LSM80-20 microelectrodes in P_{O_2} of 0.2 atm at 800°C. As grain boundaries in LSM were reported to have ~10^5 higher diffusivity than bulk LSM,[2] it was proposed that LSM thin-film microelectrodes prepared by sputtering and annealing, which have nanometer-scale columnar grains with a width in the range of ~20–70 nm,[27] have much enhanced oxygen-ion diffusion relative to bulk LSM. Therefore, LSM80-20 microelectrodes with a thickness of 65 nm can have the kinetics of ORR governed by surface oxygen exchange.

Representative EIS data collected from LSF80-20 microelectrodes with a thickness of 110 nm at 750°C are shown in Fig. 4a, where a single semicircle impedance response was found at low frequencies. Similar to LSM80-20, both real impedance and peak frequency were noted to decrease and increase with increasing P_{O_2} from 10^{-5} to 1 atm, as shown in Fig. 4a and b, respectively. This observation suggests that ORR kinetics on LSF80-20 (110 nm) is limited by surface oxygen exchange, which is in good agreement with the critical thickness reported for bulk LSF (~80 μm at 720°C).[35] The overall real impedance of LSF80-20 microelectrodes was smaller than that of LSM80-20 at all P_{O_2} levels, which was expected as oxygen-ion diffusion in LSF80-20 was much greater than that in LSM.[36,37] However, the peak frequencies found for LSF80-20, shown in Fig. 4b, were in the range from ~1 Hz at P_{O_2} = 1 atm to ~ 2 mHz at $P_{O_2} = 10^{-5}$ atm, which was considerably lower than those of LSM80-20 (5–10 times).

Estimation of oxygen surface exchange coefficients from ORR impedance data.— The k^q and k_{chem} of LSM80-20 and LSF80-20 microelectrodes were obtained from EIS data as a function of P_{O_2} and temperature. k^q was determined using the expression reported previously[24,38]

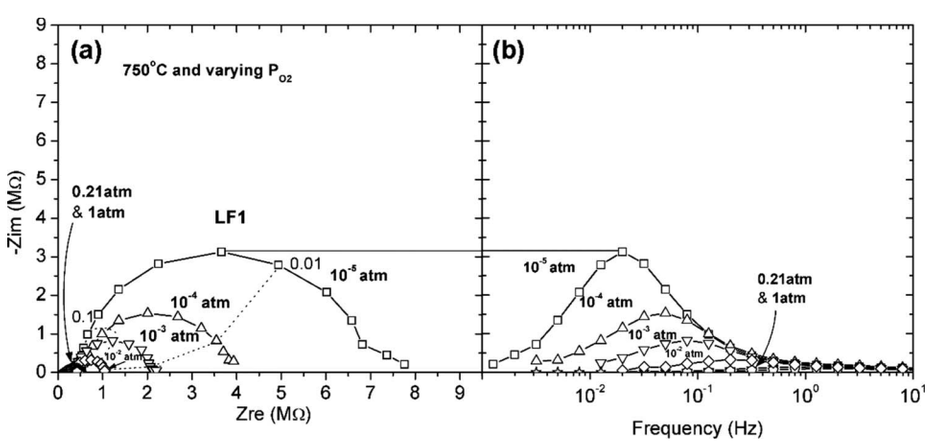

Figure 4. (a) Typical EIS spectra at 750°C from LSF80-20 microelectrode, ~170 μm in size and 110 nm thick showing the variation of impedance with different P_{O_2} from 10^{-5} to 1 atm. (b) Plot of $-Z_{im}$ vs frequency showing the change in peak frequency as a function of P_{O_2} for LSF80-20. At P_{O_2} = 1 atm, the peak frequency approaches 1 Hz. At P_{O_2} = 10^{-5} atm, the peak frequency approaches 2 mHz. Both the magnitude of impedance and the peak frequency of LSF80-20 in the entire P_{O_2} range are lower than those of LSM80-20.

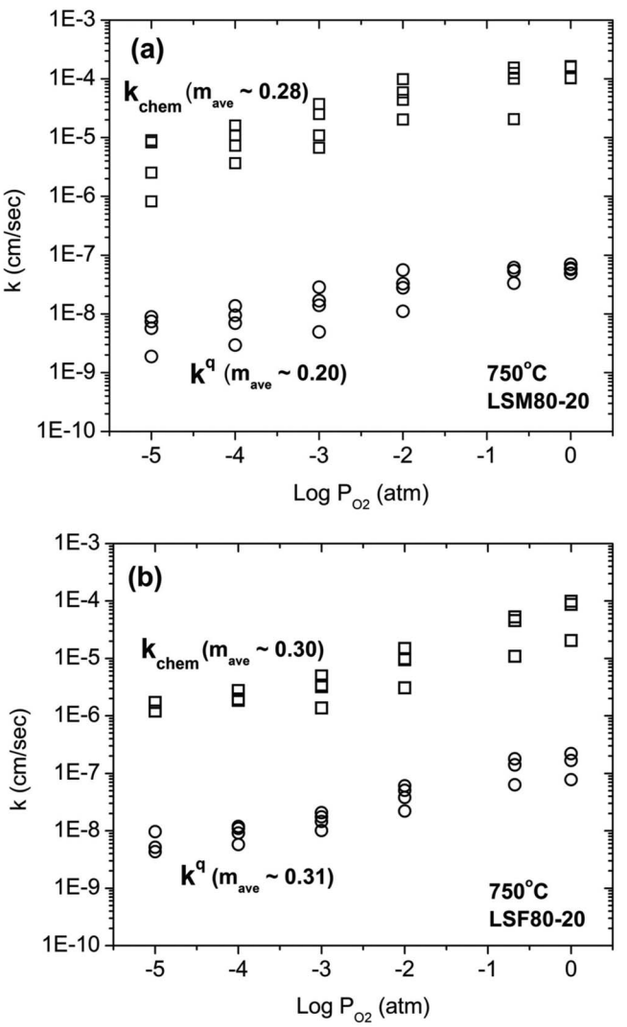

Figure 5. Calculated surface exchange coefficients, k^q and k_{chem}, in the P_{O_2} range from 10^{-5} to 1 atm at 750°C for (a) 65 nm thick LSM80-20 and (b) 110 nm thick LSF80-20. Microelectrode sizes tested here range from ~130 to ~ 190 μm. Data collected from four different microelectrodes were included to ensure data reproducibility. The slope dependence (m) of k^q and k_{chem} vs P_{O_2} for LSM80-20 was $m_{kq} \sim 0.20$ and $m_{kchem} \sim 0.28$. The slope dependence for LSF80-20 was $m_{kq} \sim 0.31$ and $m_{kchem} \sim 0.30$.

$$k^q = \frac{k_B T}{4e^2 R_s c_o} \quad [1]$$

where k_B is Boltzmann's constant, T is the absolute temperature, e is the elementary charge, R_s is the area-specific resistance for surface reaction (R_s = electrode area × R_{LF1}), and c_o is the concentration of lattice oxygen. k_{chem} was determined using the expression reported previously by Yang et al.[14]

$$k_{chem} = \frac{l}{\tau} \quad [2]$$

where l is the film thickness and τ is the relaxation time constant of the oxygen surface exchange, which is equal to the reciprocal of the peak frequency of the LF1 semicircle.

k^q values of LSM80-20 microelectrodes ranging from ~140 to ~ 190 μm with a thickness of 65 nm are shown in Fig. 5a as a function of P_{O_2} at 750°C. Average k^q values of LSM80-20 range from ~5 × 10^{-9} cm/s at 1 × 10^{-5} atm to ~ 6 × 10^{-8} cm/s at 1 atm. As k^q is approximately equivalent to the tracer surface exchange coefficient ($k^q \approx k^*$),[25] we can compare these k^q values of LSM80-20 from EIS measurements with available k^* values[2,15] of bulk LSM from IEDP/SIMS analysis. At P_{O_2} equal to and lower than 10^{-2} atm, the k^q values of LSM80-20 microelectrodes are in good agreement with k^* values (~1 × 10^{-8} cm/s at 750°C at 1 × 10^{-3} atm) of bulk LSM estimated from previous studies[2,15] provided that an activation energy of 1.32 ± 0.2 eV for k^* was used for this P_{O_2} range. However, the k^q value of LSM80-20 (~5 × 10^{-8} cm/s) at 1 atm found in this study was higher than the k^* values[2,15] of bulk LSM (in the range from 1 × 10^{-8} to 1 × 10^{-9} cm/s between 700 and 800°C). It was hypothesized that the k^q values of LSM80-20 microelectrodes in this study were higher than k^* of bulk LSM. This increase can be attributed to (*i*) underestimation of k^* values and large errors[19] in k^* values at P_{O_2} greater than 10^{-3} atm in previous IEDP/SIMS[2,19] studies as the oxygen stoichiometry of LSM80-20 is insensitive to changes in P_{O_2} in this P_{O_2} range; (*ii*) nanometer-scale microstructure (grains in the range of 20–70 nm) in the LSM80-20 microelectrodes can result in higher k^* values than bulk LSM80-20, which is supported by the fact that grain boundaries in LSM have ~10^5 higher diffusivity than bulk LSM, and there is a strong correlation that exists between D^* and k^*;[2,15] and (*iii*) different surface chemistries of LSM80-20 that can strongly affect the surface exchange rates.[31,33] The average k^q (4 × 10^{-8} cm/s) of LSM80-20 in air at 750°C is higher than that obtained from a very recent study on thin-film LSM80-20 microelectrodes (4 × 10^{-9} cm/s) in air at approximately 800°C from EIS measurements.[34] The difference in the surface oxygen exchange rate may be attributed to (*i*) dissimilar surface LSM80-20 chemistries and (*ii*) different strains for LSM80-20 thin films used in a previous study from this work.

k^q values of LSF80-20 microelectrodes ranging in size from ~130 to ~ 170 μm and with a thickness of 110 nm are shown in Fig. 5b as a function of P_{O_2} at 750°C. Average k^q values (~5 × 10^{-9} cm/s at 10^{-5} atm to ~ 2 × 10^{-7} cm/s at 1 atm) obtained for LSF80-20 microelectrodes were in agreement with those from previous IEDP/SIMS studies of bulk LSF80-20[35] having k^* in the range from ~1 × 10^{-7} to ~ 5 × 10^{-7} cm/s between 700 and 850°C at 1 atm. k^q values of LSF80-20 were found to be comparable to those of LSM80-20 found in this study. It has been proposed[19] that the electronic properties of oxides play a stronger role in determining the magnitude of surface exchange. Previous studies[21,39-41] have shown that the electronic conductivity of LSF is slightly lower than that of LSM with Sr content in the range from $x = 0.2$ to $x = 0.3$. The oxygen-ion diffusivity in LSF single crystals[22] with Sr content between 0.1 and 0.25 is over 4 orders of magnitude higher than LSM80-20.[2] Therefore, the results in this study support the hypothesis proposed by De Souza,[19] where the surface exchange coefficient such as k^* can be influenced more by the electronic properties than by ionic conductivity.

Chemical surface oxygen exchange rates, k_{chem}, of LSM80-20 microelectrodes, which were determined from Eq. 2, were found to be similar to or slightly higher than those of LSF80-20, as shown in Fig. 5a and b, respectively. As expected, the k_{chem} values were much greater than the k^q and k^* values discussed above. Using the experimentally determined k^q and k_{chem} values of LSM80-20 and LSF80-20 microelectrodes, the thermodynamic enhancement factor γ can be calculated from $\gamma = k_{chem}/k^q$ [42] as a function of P_{O_2}. The values of γ averaged over multiple data sets of LSM80-20 (four sets) and LSF80-20 (three sets) shown in Fig. 5a and b at each P_{O_2} are shown in Fig. 6a. γ was found to be in the range from ~1000 to ~4500 for LSM80-20 between 10^{-5} and 1 atm at 750°C, where γ appeared to increase with increasing P_{O_2} from 10^{-5} to 10^{-2} atm and was relatively constant at 10^{-2} atm and higher. In contrast, smaller γ values from ~200 to ~400 were observed for LSF80-20 in the same P_{O_2} range and at the same temperature, where γ appeared to be constant from 10^{-5} to 10^{-2} atm and increased with P_{O_2} at

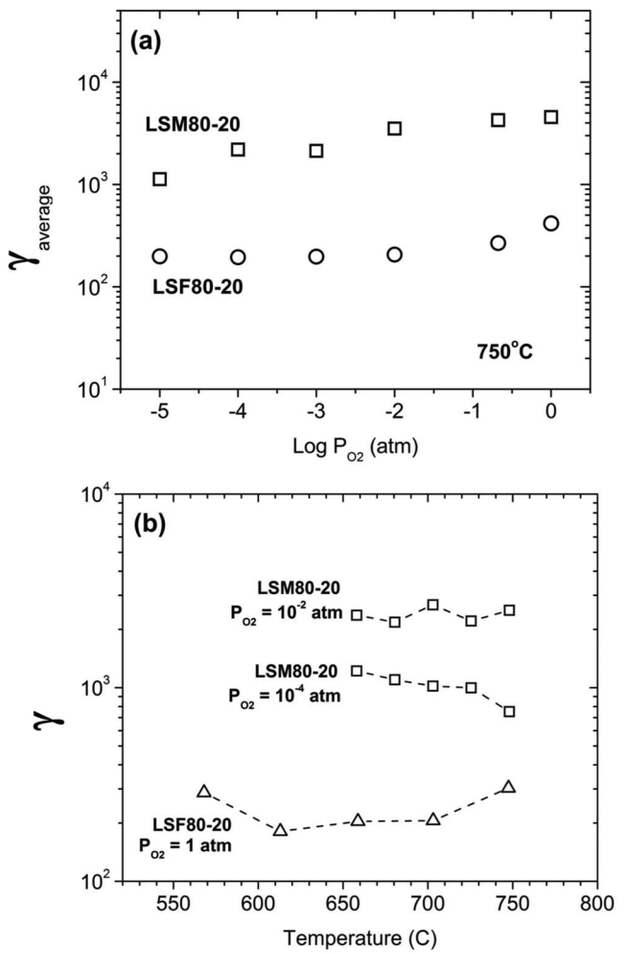

Figure 6. (a) Thermodynamic enhancement factor (γ) as a function of P_{O_2} for 65 nm thick LSM80-20 and 110 nm thick LSF80-20 at 750°C. γ was calculated by taking the ratio of k_{chem}/k^q using four data sets of LSM80-20 and three data sets of LSF80-20 (shown in Fig. 5a and b). Microelectrodes ranging in size from ~130 to ~ 190 μm were tested between P_{O_2} of 10^{-5} and 1 atm. γ for LSM80-20 was found to range from ~1000 to ~4500, while γ for LSF80-20 was found to range between ~200 and ~400. (b) Thermodynamic factor (γ) obtained from single data sets for LSM80-20 as a function of temperature between 570 and 750°C at P_{O_2} of 10^{-4} and 10^{-2} atm and for LSF80-20 at P_{O_2} of 1 atm. γ was found to range between ~200 and ~300 for LSF80-20 and between ~700 and ~3000 for LSM80-20 in the temperature range examined.

10^{-2} atm and higher. The temperature dependence of γ values for LSM80-20 at P_{O_2} of 10^{-4} and 10^{-2} atm and for LSF80-20 at P_{O_2} of 1 atm is presented in Fig. 6b. γ for both materials does not vary greatly as a function of temperature. This study provides a direct report of γ values for LSM80-20 and LSF80-20 obtained from EIS measurements.

The γ values obtained from this study can be compared with those extracted from thermogravimetric data reported previously using Eq. 3

$$\gamma = \frac{1}{2RT}\frac{\partial(\mu_{O_2})}{\partial \ln c_O} = \frac{1}{2}\frac{\partial \ln P_{O_2}}{\partial \ln c_O} \quad [3]$$

where R and T are the gas constant and temperature in Kelvin, respectively, μ_{O_2} is the chemical potential of oxygen, c_o is the concentration of oxide ions, and P_{O_2} is the oxygen partial pressure. Using the thermogravimetric data of LSM80-20,[43] γ was estimated to range from ~270 to ~2400 in the P_{O_2} range from 10^{-5} to 1 atm at 800°C. γ values of $La_{0.75}Sr_{0.25}FeO_3$ [44] fall in the range from ~70 to ~160 in the P_{O_2} range from 10^{-5} to 1 atm at 800°C, and which were consistent with γ values of typical MIEC oxides.[4,14] Because c_o is fairly constant over a wider range of P_{O_2} for LSM80-20 [43] in comparison to $La_{0.75}Sr_{0.25}FeO_3$,[44] higher γ values are therefore expected for LSM80-20. γ values of LSM80-20 obtained from EIS measurements in this study were in reasonable agreement with those extracted from previously reported thermogravimetric data,[43] while those of LSF80-20 microelectrodes obtained in this study were higher than those based on thermogravimetric data,[44] which may be attributed to Fe deficiency in the LSF80-20 microelectrodes (Table I).

Oxygen partial pressure dependence of surface oxygen exchange coefficients.— Examination of the dependence (m) of P_{O_2} on surface exchange coefficients (k^q,$k_{chem} \propto P_{O_2}^m$) can provide insights into the species involved in the rate-limiting step for surface oxygen exchange.[4,14,45,46] The k^q and k_{chem} values of LSM80-20 shown in Fig. 5a increase with increasing P_{O_2}, having a dependence of m_{k^q} = 0.20 and $m_{k_{chem}}$ = 0.28 in the P_{O_2} range from 10^{-5} to 1 atm, respectively. There is no reliable P_{O_2} dependence of surface exchange on bulk LSM80-20 from previous isotope studies[19] due to the large errors in k^* at high P_{O_2}. The P_{O_2} dependence of $\sim\frac{1}{2}$ for k^q in the range of 10^{-4}–10^{-2} atm can be estimated from the results of LSM80-20 microelectrodes (250 nm) reported by Fleig et al.,[34] which were considerably higher than that (~0.25) of our electrodes in the same P_{O_2} range. Similarly, the k^q and k_{chem} values of LSF80-20 presented in Fig. 5b have a P_{O_2} dependence of m_{k^q} = 0.31 and $m_{k_{chem}}$ = 0.30 in the P_{O_2} range from 10^{-5} to 1 atm, respectively. The observed P_{O_2} dependence in this study was considerably lower than those reported by ten Elshof et al.,[45] where $m_{k_{chem}}$ = 0.75–0.95 and m_{k^q} = 0.65–0.85 have been noted for LSF (x_{Sr} = 0.1 and 0.4), and the dependencies do not change greatly with Sr content nor with temperature in the range from 650 to 950°C. However, the P_{O_2} dependence of LSF (x_{Sr} = 0.5) reported by Yoo et al.[47] varied from m = 0.21 to m = 0.51 for k_{chem} in the P_{O_2} range from 10^{-2} to 5×10^{-1} atm between 780 and 950°C, which cannot be explained consistently by the work of ten Elshof et al.[45] due to the compositional similarity of LSF (x_{Sr} = 0.5 vs 0.4). The P_{O_2} dependence of ORR polarization ($R \propto P_{O_2}^m$) can be related to the oxygen species involved in the rate-limiting reaction. Consider the following three processes,[48-50] where

$$m = 1 \quad O_{2,gas} \leftrightarrow O_{2,ads} \quad [4]$$

$$m = \tfrac{1}{2} \quad O_{2,ads} \leftrightarrow 2O_{ads} \quad [5]$$

$$m = \tfrac{1}{4} \quad O_{ads} + 2e^- + V_O \leftrightarrow O_o^x \quad [6]$$

Using this simple model, charge transfer with incorporation (Eq. 6) may be considered as the rate-limiting step for surface oxygen exchange on LSM80-20 and LSF80-20. However, this assignment is not unique as many elementary reaction steps can give rise to a P_{O_2} dependence of $\frac{1}{4}$.

Here we discuss the observed P_{O_2} dependence of k^q in the context of three recently proposed mechanisms for oxygen surface exchange, which provides some insights into the underlying rate-limiting step of surface exchange. First, De Souza[19] derived an empirical, atomistic expression for k^* based on the P_{O_2} dependence for electron-poor materials ($m \sim 0.23$) such as $La_{0.9}Sr_{0.1}Ga_{0.8}Mg_{0.2}O_{2.85}$ and for electron-rich materials ($m \sim 0.39$) such as LSCF, where the charge transfer of one electron to an adsorbed oxygen was considered as the rate-limiting step for both types of materials. The observed P_{O_2} dependence of LSM80-20 ($m \sim 0.20$) at 750°C in this study was considerably lower than that

($m \sim 0.46$) predicted for LSM80-20 at 1000°C by De Souza[19] based on limited data at P_{O_2} equal to and lower than 10^{-2} atm. Although the observed P_{O_2} dependence of LSM80-20 ($m \sim 0.20$) was close to that of electron-poor materials in this model, LSM80-20 is known to have high electronic conductivity,[41] and microprobes placed on two different locations on the LSM80-20 microelectrodes of this study show very small resistance. Therefore, the observed P_{O_2} dependence of k^q for LSM80-20 as well as that for LSF80-20 ($m = \sim 0.30$) cannot be explained consistently by the model of De Souza.[19] Second, Adler et al.[20] modeled the experimental P_{O_2} dependence of the chemical surface exchange rate (k_{chem}) of metallic LSC (having $x = 0.2$, 0.5, and 0.7) from the data of van der Haar et al.,[51] with m in the range from ~0.43 to ~0.92, from which a dissociative adsorption step was proposed as rate-limiting. For p-type semiconductors such as LSF, a chemisorption limitation or barrier to charge transfer is considered as the rate-limiting step in the range from $m \sim 0.75$ to $m \sim 0.95$ based on the experimental data of LSF ($x = 0.1$ and 0.4) from ten Elshof et al.[45] The observed P_{O_2} dependence of k^q for LSM80-20 found in this study was too low for those expected for metallic and p-type semiconductor MIEC cathodes. The observed P_{O_2} dependence of k^q for LSF80-20 ($m = \sim 0.30$) in this study was considerably lower than those of LSF ($x_{Sr} = 0.1$ and 0.4) reported by ten Elshof et al.,[45] but comparable to that of LSF ($x_{Sr} = 0.5$) reported by Yoo et al.[47] Therefore, the P_{O_2} dependence of k^q for LSF80-20 microelectrodes cannot be compared consistently with the model reported for p-type semiconductors.[20] Fe deficiency in the LSF80-20 microelectrodes may influence the P_{O_2} dependence of k^q, the extent of which is not understood. Third, Fleig et al.[26] showed that the rate-limiting steps of electron transfer such as $O_{ad} + e^- \rightarrow O_{ad}^-$ and $O_{ad}^- + e^- \rightarrow O_{ad}^{2-}$ can give rise to P_{O_2} dependence of $\frac{1}{4}$ in the P_{O_2} range from 10^{-5} to 1 atm at 1000 K, which corresponds to a high coverage of O_{ad}^- or $O_{2,ad}^{2-}$ on materials with P_{O_2}-independent hole concentrations. As the observed P_{O_2} dependence of LSM80-20 is close to $\frac{1}{4}$ and LSM80-20 has a P_{O_2}-independent hole concentration above 10^{-10} atm at 800°C,[41] it was hypothesized in this study that the electron transfer such as $O_{ad} + e^- \rightarrow O_{ad}^-$ and $O_{ad}^- + e^- \rightarrow O_{ad}^{2-}$ can be rate-limiting for surface oxygen exchange on LSM80-20 microelectrodes. This previous study[26] showed that a rate-limiting step of electron transfer to form O_{ad}^- or $O_{2,ad}^{2-}$ can give rise to a P_{O_2} dependence of $\sim\frac{3}{8}$ for materials having electronic carrier concentrations with P_{O_2} dependence of $\frac{1}{4}$ in the P_{O_2} range from 10^{-5} to 1 atm at 1000 K. Because the observed P_{O_2} dependence of k^q for LSF80-20 ($m = \sim 0.30$) was between $\frac{1}{4}$ and $\frac{3}{8}$, and LSF80-20 has an $\sim\frac{1}{4}$ P_{O_2}-dependent hole concentration below 1 atm at 800°C,[39] it was proposed here that the electron transfer to form O_{ad}^- or $O_{2,ad}^{2-}$ can be rate-limiting for surface oxygen exchange on LSF80-20. Further studies are needed to test these hypotheses on the proposed rate-limiting step on LSM80-20 and LSF80-20.

Temperature dependence of surface exchange coefficients.— The temperature dependence of k^q and k_{chem} for LSM80-20 was examined in the range between 660 and 770°C at two P_{O_2} levels (10^{-2} and 10^{-4} atm), as shown in Fig. 7a. The activation energy (E_a) for k^q of LSM80-20 was 1.87 ± 0.02 and 2.01 ± 0.02 eV at 10^{-4} and 10^{-2} atm, respectively. The E_a of k_{chem}, in contrast, was 1.48 ± 0.01 and 2.06 ± 0.04 eV at 10^{-4} and 10^{-2} atm, respectively. Previously De Souza et al.[2,15] showed that the E_a of k^* in LSM80-20 is equal to 1.33 ± 0.20 eV between 700 and 1000°C at 1 atm. However, large errors and underestimation in k^* values for LSM80-20 at a P_{O_2} greater than 10^{-3} atm from the IEDP/SIMS measurements[2,19] led to ambiguity in the reported activation energy. E_a values for k^q in this study were in good agreement with a hypothesis proposed by De Souza et al.,[15] where E_a for k^* falls in the range from 0.4 to 0.7E_a of D^* (~2.6–3.0 eV) in LSM.[2,18]

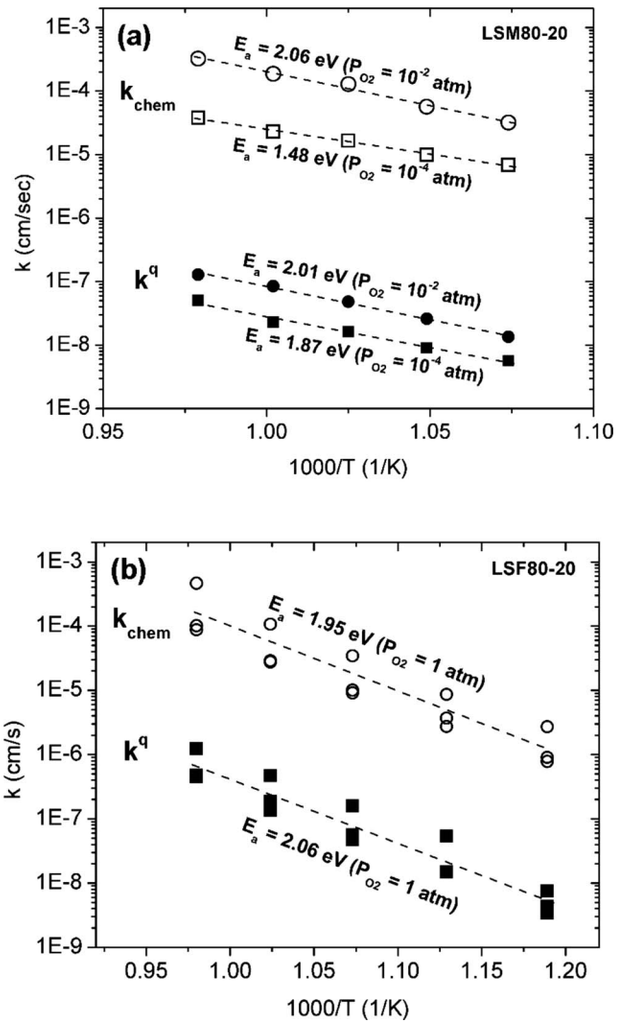

Figure 7. Calculated surface exchange coefficients, k^q and k_{chem}, for (a) LSM80-20, ~190 μm in size and 65 nm thick, between 770 and 660°C at two P_{O_2} levels of 10^{-2} and 10^{-4} atm. Activation energy for k^q increases from 1.87 to 2.01 eV with increasing P_{O_2}. Activation energy for k_{chem} also increased from 2.06 to 1.48 eV with increasing P_{O_2}. (b) Calculated surface exchange coefficients, k^q and k_{chem}, for LSF80-20 obtained from three data sets, ~170 μm in size and 110 nm thick, between 770 and 570°C at 1 atm P_{O_2}. Activation energies for k^q and k_{chem} were 2.06 and 1.95 eV, respectively.

E_a values of k_{chem} and k^q for LSF80-20 microelectrodes were 1.95 ± 0.02 and 2.06 ± 0.02 eV between 570 and 750°C at 1 atm of P_{O_2}, respectively, as shown in Fig. 7b. These activation energy values are comparable to those of $La_{0.6}Sr_{0.4}FeO_3$ thin-film microelectrodes reported previously.[52] However, these values are considerably higher than those of bulk LSF reported by Petitjean et al.,[35] who reported that a temperature dependence of k^* on bulk LSF80-20 and an E_a value of ~1 eV can be estimated from the data collected at $P_{O_2} = 0.2$ atm. A wide range of scatter exists in the previously reported E_a of k^* and k_{chem} for bulk LSF. ten Elshof et al.[45] previously reported E_a values of 1.17 ± 0.2 and 1.36 ± 0.4 eV for k^* on $La_{0.9}Sr_{0.1}FeO_3$ and $La_{0.6}Sr_{0.4}FeO_3$ at $P_{O_2} = 10^{-3}$ atm, respectively. However, Søgaard et al.[46] reported an E_a of 2.06 ± 0.2 eV for k_{chem} and an E_a of 1.79 ± 0.35 eV for k^* on $La_{0.6}Sr_{0.4}FeO_3$ at $P_{O_2} = 8.7 \times 10^{-4}$ atm. The physical origin of the scatter of activation energies for k^* and k_{chem} of bulk LSF is not clearly understood.

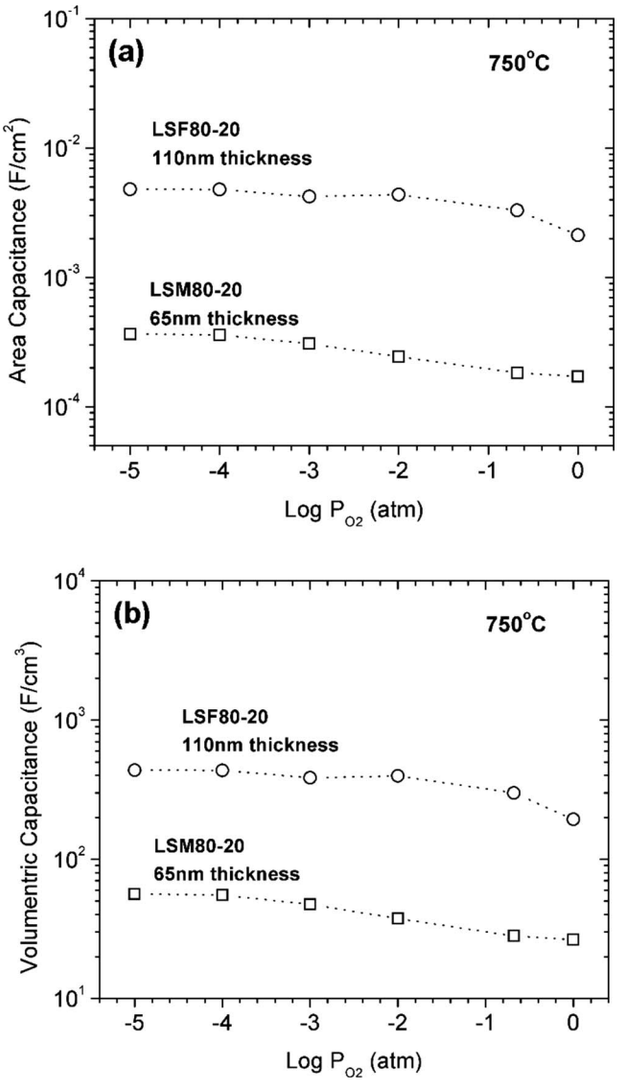

Figure 8. (a) Chemical capacitance per unit area (F/cm^2) for 65 nm thick LSM80-20 and 110 nm thick LSF80-20 as a function of P_{O_2}. Microelectrode sizes tested here ranged from ~130 to ~ 190 μm. (b) Chemical capacitance per unit volume (F/cm^3) for LSM80-20 and LSF80-20 thin-film electrodes as a function of P_{O_2}. LSF80-20, with almost double the microelectrode thickness, had chemical capacitance values almost 1 order of magnitude larger than LSM80-20 in the entire range of P_{O_2}. Because oxygen vacancy concentration in LSF80-20 is inherently greater than LSM80-20, a higher chemical capacitance for the ferrite-based film is therefore expected.

Chemical capacitance estimated from ORR impedance data.— As the magnitude of chemical capacitance provides a good measure of bulk oxide involvement and, therefore, an indication of increased oxygen vacancy content,[53] the chemical capacitance per unit area (F/cm^2) and per unit volume (F/cm^3) for LSM80-20 and LSF80-20 films was determined as a function of P_{O_2} at 750°C, as shown in Fig. 8a and b, respectively. These values were calculated from the expression by Fleig[54]

$$C = (R_{LF1}^{1-p}\chi)^{1/p} \quad [7]$$

where R_{LF1} is the parallel resistance value in the equivalent circuit, χ is the nonideal "capacitance," and p is the nonideality factor used to fit the CPE. The area-specific and volumetric chemical capacitances of LSM80-20 at 750°C were fairly constant over the entire P_{O_2} range and slightly decreased (5×10^{-4}–2×10^{-4} F/cm^2 for area-specific capacitance vs 6×10^{1}–3×10^{1} F/cm^3 for volumetric capacitance) with increasing P_{O_2} from 10^{-5} to 1 atm. These results are in good agreement with those of LSM80-20 microelectrodes, with a thickness of 250 nm, previously reported (~5×10^{-4} F/cm^2 for area-specific capacitance vs ~2×10^{1} F/cm^3 for volumetric capacitance) in the P_{O_2} range from 5×10^{-4} to 1 atm at ~800°C.[34]

As expected from the oxygen nonstoichiometry of LSM80-20 and LSF80-20 as a function of P_{O_2},[43,44] the area-specific (5×10^{-3}–2×10^{-3} F/cm^2) and volumetric (4×10^{2}–2×10^{2} F/cm^3) chemical capacitances for LSF80-20, despite its almost doubled microelectrode thickness, are approximately 1 order of magnitude greater than those for LSM80-20 at 750°C. A similar trend in the area-specific and volumetric capacitances as a function of P_{O_2} for LSM80-20 was found for LSF80-20, which showed that the capacitances also slightly decreased with increasing P_{O_2} from 10^{-5} to 1 atm. The area-specific and volumetric capacitance values of this study are approximately 1 order of magnitude smaller than those reported for 100 nm thick LSF ($x_{Sr} = 0.4$) microelectrodes at 750°C in air reported by Baumann et al.[52] (1.2×10^{-2} F/cm^2 for area-specific capacitance and 1.5×10^{3} F/cm^3 for volumetric capacitance). The reduced capacitance observed with LSF80-20 can be attributed to the lower Sr content in LSF80-20 relative to LSF ($x_{Sr} = 0.4$), which decreases the inherent oxygen vacancy concentration in the perovskite.[44]

The volume-specific chemical capacitance ($C = (8F^2/V_mRT)d\delta/d \ln P_{O_2}$, where V_m is the molar volume of the oxide) estimated from thermogravimetric data of bulk LSM80-20 and LSF80-20 previously reported[43,44] ranges from 200–1600 F/cm^3 and 2000–4000 F/cm^3, respectively, in the P_{O_2} range measured in this study. These values are approximately 1 order of magnitude higher than those for the thin-film LSM80-20 and LSF80-20 microelectrodes of this study. A reduction in the volume-specific capacitance and oxygen vacancy concentration in thin-film LSC microelectrodes relative to bulk LSC has been observed previously.[55] It was proposed that the compressive strains and nanograins present in the 65 nm thick LSM80-20 microelectrodes of this study can modify the thermodynamic parameters and thus reduce the chemical capacitance of these microelectrodes relative to bulk LSM80-20, while the Fe deficiency and compressive strains and nanograins present in the 110 nm thick LSF80-20 microelectrodes may contribute to chemical capacitance reduction relative to bulk LSF80-20.

Conclusions

The EIS data of dense, thin-film LSM80-20 and LSF80-20 microelectrodes have been used to determine the (*i*) electrical (k^q) and chemical (k_{chem}) surface oxygen exchange coefficients, (*ii*) thermodynamic enhancement factor (γ), and (*iii*) chemical capacitance as a function of P_{O_2} and temperature. While the oxygen-ion conductivity in bulk LSM80-20 is low, LSM microelectrodes with a thickness of 65 nm and nanometer-scale microstructure showed enhanced ion transport relative to bulk LSM, where ORR kinetics is limited by surface oxygen exchange. We demonstrated that k^q and k_{chem} on LSM80-20 at $P_{O_2} > 10^{-2}$ atm can be measured accurately in contrast to large errors in k^* from conventional tracer measurements. Moreover, although the chemical capacitance for LSF80-20 is greater than that for LSM80-20, indicating a higher oxygen vacancy concentration for the iron-based perovskite, k^q and k_{chem} of LSM80-20 and LSF80-20 microelectrodes are shown to be comparable, which reveals the potential importance of electronic properties over oxygen vacancy content in determining the magnitude of surface oxygen exchange. The P_{O_2} dependence of k^q and k_{chem} of LSM80-20 and LSF80-20 microelectrodes falls in the range from ~0.2 to ~0.3. This suggests a common rate-limiting reaction for surface oxygen exchange, namely, electron transfer to an adsorbed oxygen species based on the work of Fleig et al.[26] Further research that combines film structural analysis, surface science, EIS, and sur-

face exchange reaction modeling is needed to determine the nature of the rate-limiting step for surface oxygen exchange.

Acknowledgments

The authors thank Harry L. Tuller for fruitful discussions and helpful suggestions. This research made use of the Shared Experimental Facilities supported by the MRSEC Program of the National Science Foundation (NSF) under award no. DMR-0819762. This work was supported in part by the NSF MRSEC Program under award no. DMR-0819762 and through an NSF grant, no. CBET-0844526.

Massachusetts Institute of Technology assisted in meeting the publication costs of this article.

References

1. H. Ullmann, N. Trofimenko, F. Tietz, D. Stover, and A. Ahmad-Khanlou, *Solid State Ionics*, **138**, 79 (2000).
2. R. A. De Souza, J. A. Kilner, and J. F. Walker, *Mater. Lett.*, **43**, 43 (2000).
3. R. A. De Souza and J. A. Kilner, *Solid State Ionics*, **106**, 175 (1998).
4. J. E. ten Elshof, M. H. R. Lankhorst, and H. J. M. Bouwmeester, *Solid State Ionics*, **99**, 15 (1997).
5. J. Mizusaki, T. Saito, and H. Tagawa, *J. Electrochem. Soc.*, **143**, 3065 (1996).
6. J. E. ten Elshof, H. J. M. Bouwmeester, and H. Verweij, *Solid State Ionics*, **81**, 97 (1995).
7. S. Carter, A. Selcuk, R. J. Chater, J. Kajda, J. A. Kilner, and B. C. H. Steele, *Solid State Ionics*, **53**, 597 (1992).
8. H. J. M. Bouwmeester, H. Kruidhof, and A. J. Burggraaf, *Solid State Ionics*, **72**, 185 (1994).
9. J. A. Kilner, R. A. De Souza, and I. C. Fullarton, *Solid State Ionics*, **86–88**, 703 (1996).
10. J. A. Lane and J. A. Kilner, *Solid State Ionics*, **136**, 997 (2000).
11. S. Kim, S. Wang, X. Chen, Y. L. Yang, N. Wu, A. Ignatiev, A. J. Jacobson, and B. Abeles, *J. Electrochem. Soc.*, **147**, 2398 (2000).
12. J. E. ten Elshof, H. J. M. Bouwmeester, and H. Verweij, *Solid State Ionics*, **89**, 81 (1996).
13. Y. L. Yang, A. J. Jacobson, C. L. Chen, G. P. Luo, K. D. Ross, and C. W. Chu, *Appl. Phys. Lett.*, **79**, 776 (2001).
14. Y. L. Yang, C. L. Chen, S. Y. Chen, C. W. Chu, and A. J. Jacobson, *J. Electrochem. Soc.*, **147**, 4001 (2000).
15. R. A. De Souza and J. A. Kilner, *Solid State Ionics*, **126**, 153 (1999).
16. E. Boehm, J. M. Bassat, P. Dordor, F. Mauvy, J. C. Grenier, and P. Stevens, *Solid State Ionics*, **176**, 2717 (2005).
17. E. Boehm, J. M. Bassat, M. C. Steil, P. Dordor, F. Mauvy, and J. C. Grenier, *Solid State Sci.*, **5**, 973 (2003).
18. I. Yasuda, K. Ogasawara, M. Hishinuma, T. Kawada, and M. Dokiya, *Solid State Ionics*, **86**, 1197 (1996).
19. R. A. De Souza, *Phys. Chem. Chem. Phys.*, **8**, 890 (2006).
20. S. B. Adler, X. Y. Chen, and J. R. Wilson, *J. Catal.*, **245**, 91 (2007).
21. O. Yamamoto, Y. Takeda, R. Kanno, and M. Noda, *Solid State Ionics*, **22**, 241 (1987).
22. T. Ishigaki, S. Yamauchi, K. Kishio, J. Mizusaki, and K. Fueki, *J. Solid State Chem.*, **73**, 179 (1988).
23. C. D. Baertsch, K. F. Jensen, J. L. Hertz, H. L. Tuller, V. T. Srikar, S. M. Spearing, and M. A. Schmidt, *J. Mater. Res.*, **19**, 2604 (2004).
24. J. Maier, *Physical Chemistry of Ionic Materials: Ions and Electrons in Solids*, p. 537, John Wiley & Sons, Chichester, England (2004).
25. J. Maier, *Solid State Ionics*, **112**, 197 (1998).
26. J. Fleig, R. Merkle, and J. Maier, *Phys. Chem. Chem. Phys.*, **9**, 2713 (2007).
27. G. J. la O', B. Yildiz, S. McEuen, and Y. Shao-Horn, *J. Electrochem. Soc.*, **154**, B427 (2007).
28. T. Hashimoto, N. Ishizawa, N. Mizutani, and M. Kato, *J. Cryst. Growth*, **84**, 207 (1987).
29. S. E. Dann, D. B. Curric, M. T. Weller, M. F. Thomas, and A. D. Al-Rawwas, *J. Solid State Chem.*, **109**, 134 (1994).
30. JCPDS Card No. 30-1468.
31. F. S. Baumann, J. Fleig, M. Konuma, U. Starke, H. U. Habermeier, and J. Maier, *J. Electrochem. Soc.*, **152**, A2074 (2005).
32. A. Endo, H. Fukunaga, C. Wen, and K. Yamada, *Solid State Ionics*, **135**, 353 (2000).
33. G. J. la O', R. F. Savinell, and Y. Shao-Horn, *J. Electrochem. Soc.*, **156**, B771 (2009).
34. J. Fleig, H. R. Kim, J. Jamnik, and J. Maier, *Fuel Cells*, **8**, 330 (2008).
35. M. Petitjean, G. Caboche, E. Siebert, L. Dessemond, and L. C. Dufour, *J. Eur. Ceram. Soc.*, **25**, 2651 (2005).
36. S. P. Simner, J. P. Shelton, M. D. Anderson, and J. W. Stevenson, *Solid State Ionics*, **161**, 11 (2003).
37. J. M. Ralph, C. Rossignol, and R. Kumar, *J. Electrochem. Soc.*, **150**, A1518 (2003).
38. J. Fleig and J. Maier, *J. Eur. Ceram. Soc.*, **24**, 1343 (2004).
39. M. V. Patrakeev, J. A. Bahteeva, E. B. Mitberg, I. A. Leonidov, V. L. Kozhevnikov, and K. R. Poeppelmeier, *J. Solid State Chem.*, **172**, 219 (2003).
40. L. W. Tai, M. M. Nasrallah, H. U. Anderson, D. M. Sparlin, and S. R. Sehlin, *Solid State Ionics*, **76**, 259 (1995).
41. J. Mizusaki, Y. Yonemura, H. Kamata, K. Ohyama, N. Mori, H. Takai, H. Tagawa, M. Dokiya, K. Naraya, and T. Sasamoto, *Solid State Ionics*, **132**, 167 (2000).
42. S. Kim, Y. L. Yang, A. J. Jacobson, and B. Abeles, *Solid State Ionics*, **121**, 31 (1999).
43. J. Mizusaki, N. Mori, H. Takai, Y. Yonemura, H. Minamiue, H. Tagawa, M. Dokiya, H. Inaba, K. Naraya, T. Sasamoto, et al., *Solid State Ionics*, **129**, 163 (2000).
44. J. Mizusaki, M. Yoshihiro, S. Yamauchi, and K. Fueki, *J. Solid State Chem.*, **58**, 257 (1985).
45. J. E. ten Elshof, M. H. R. Lankhorst, and H. J. M. Bouwmeester, *J. Electrochem. Soc.*, **144**, 1060 (1997).
46. M. Søgaard, P. Vang Hendriksen, and M. Mogensen, *J. Solid State Chem.*, **180**, 1489 (2007).
47. J. Yoo, A. Verma, S. Wang, and A. J. Jacobson, *J. Electrochem. Soc.*, **152**, A497 (2005).
48. D. Y. Wang and A. S. Nowick, *J. Electrochem. Soc.*, **126**, 1155 (1979).
49. Y. Takeda, R. Kanno, M. Noda, Y. Tomida, and O. Yamamoto, *J. Electrochem. Soc.*, **134**, 2656 (1987).
50. E. Siebert, A. Hammouche, and M. Kleitz, *Electrochim. Acta*, **40**, 1741 (1995).
51. L. M. van der Haar, M. W. den Otter, M. Morskate, H. J. M. Bouwmeester, and H. Verweij, *J. Electrochem. Soc.*, **149**, J41 (2002).
52. F. S. Baumann, J. Fleig, G. Cristiani, B. Stuhlhofer, H. U. Habermeier, and J. Maier, *J. Electrochem. Soc.*, **154**, B931 (2007).
53. S. Adler, *Chem. Rev. (Washington, D.C.)*, **104**, 4971 (2004).
54. J. Fleig, *Solid State Ionics*, **150**, 181 (2002).
55. T. Kawada, J. Suzuki, M. Sase, A. Kaimai, K. Yashiro, Y. Nigara, J. Mizusaki, K. Kawamura, and H. Yugami, *J. Electrochem. Soc.*, **149**, E252 (2002).